Auxiliary Material for

Buoyant currents arrested by convective dissolution

Christopher W. MacMinn and Ruben Juanes

Materials and Methods

Analog fluid system. We work with analogue fluids rather than CO_2 and water to allow experiments at room temperature and pressure, where the solubility of CO_2 in water is extremely low ($\sim 0.15\%$ by mass) and the density and viscosity of CO_2 are much lower than at reservoir conditions. In order to conduct experiments with and without convective dissolution, we use two different pairs of analogue fluids.

In the analogue system with convective dissolution, water plays the role of the buoyant CO_2 and propylene glycol (PG) plays the role of the denser and more viscous ambient groundwater [1]. Although pure PG is denser than water ($\Delta\rho \approx 36\,\mathrm{kg/m^3}$), the density of water-PG mixtures is non-monotonic with water concentration and mixtures of the two with up to about 54% water are denser than pure PG [Fig. S1(a)]. As a result, a layer of water will float above a layer of PG while simultaneously dissolving into the PG by convective dissolution, as fingers of the dense mixture that forms at the interface between the two sink downward into the PG [Fig. S1(c)].

To study buoyant currents without convective dissolution, we replace the PG with a mixture of glycerol and water. All such mixtures are denser and more viscous than water. We choose one for which the viscosity contrast is similar to the water-PG system (77.5% glycerol by mass, for which $\Delta\rho \approx 200\,\mathrm{kg/m^3}$ and $\mathcal{M} \approx 40$) [Fig. S1(b)]. As in the water-PG system, the buoyant water will mix with the dense glycerol-water mixture along their shared interface. Unlike in the water-PG system, this will never trigger convective dissolution because the density of water-glycerol mixtures is monotonic in water concentration.

With these two fluid pairs, we are able to study buoyant currents with and without convective dissolution while keeping other parameters approximately constant. In both systems, we add a small amount of blue food dye to the water for visualization.

Flow cell and experimental procedure. We conduct experiments in a quasi-two-dimensional flow cell packed with spherical glass beads. The cell is constructed from three pieces of laser-cut acrylic—solid front and rear panels, and a middle spacer that frames the working area. The working area is 5.2 cm tall, 56 cm long, and about 1 cm thick. The spacer is held tightly between the front and rear panels via bolts. Once assembled, we orient the cell "vertically" (long direction aligned with gravity) and fill it with glass beads via a port. We tap the cell vigorously during filling to generate a tight, consistent bead pack. Once the cell is full, we plug this port.

For simplicity, we work with only one bead size: spherical beads with a nominal mean diameter of $1.25\,\mathrm{mm}$. We use soda-lime glass spheres from Mo-Sci Specialty Products, LLC, with a nominal

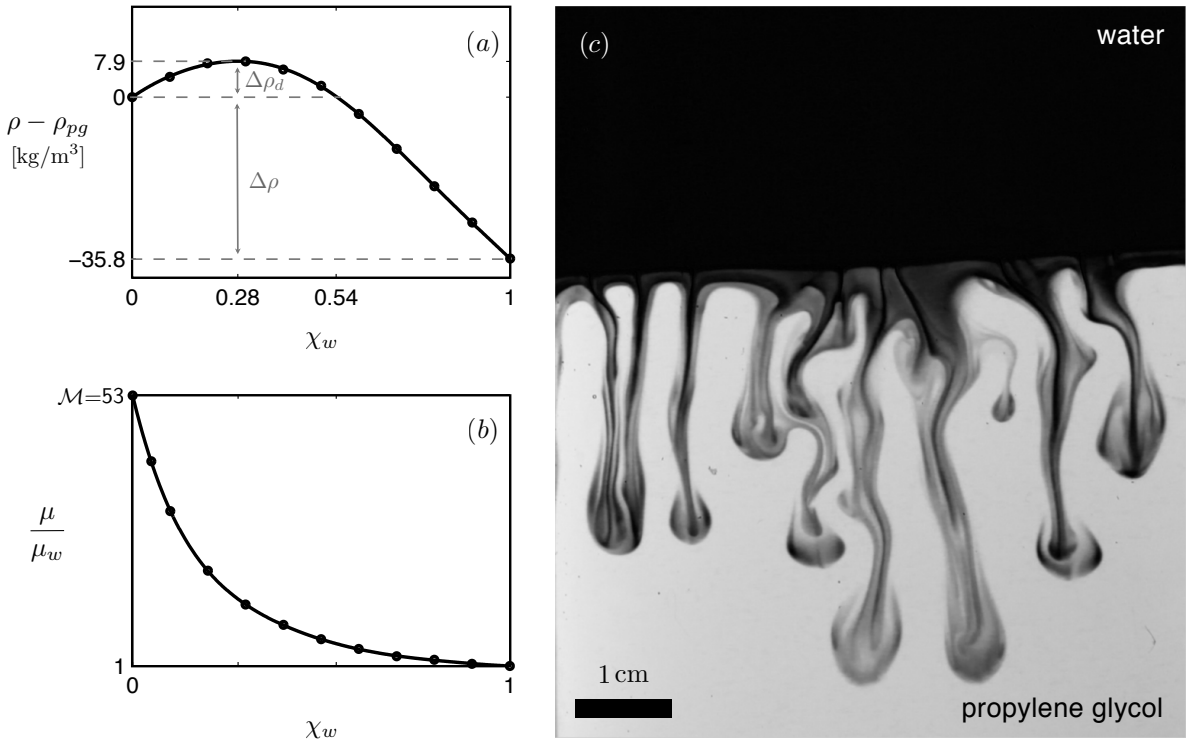

Figure S1. (color online). We study buoyant currents with convective dissolution using analogue fluids: water and propylene glycol (PG). Pure PG is denser and more viscous than water, but a mixture of the two is denser than either component for water mass fractions less than about 0.54, and this drives convective dissolution [1]. Here we show (a) the amount by which the density of the mixture exceeds the density of pure PG, (b) the ratio of the viscosity of the mixture to the viscosity of pure water (circles are experimental measurements at $25\,^\circ$C [2; 3] and solid lines are polynomial fits to the data), and (c) a snapshot from an experiment in a Hele-Shaw cell where a layer of buoyant water floats above a layer of denser PG while dissolving into PG via convective dissolution.

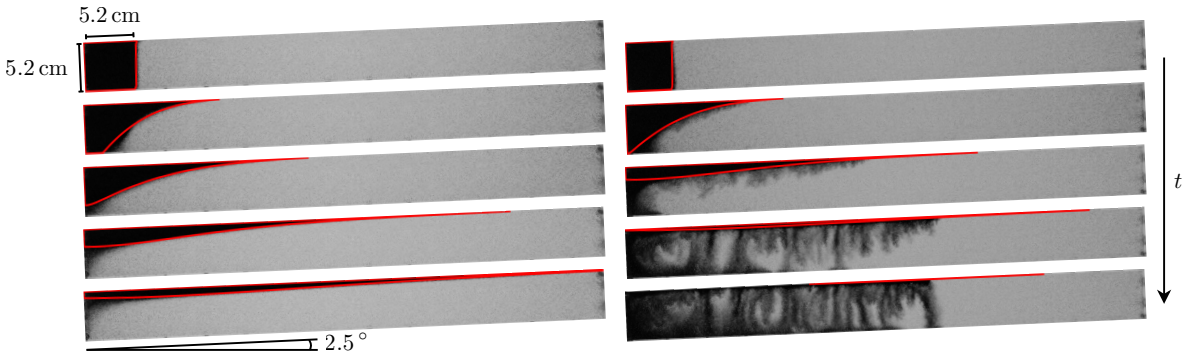

Figure S2. (color online) Snapshots of experiments in the flow cell packed with glass beads. Left: a buoyant current of water (dark) migrates over glycerol and water. Right: a buoyant current of water (dark) migrates over PG while dissolving via convective dissolution. We superpose the predictions of the model (red lines) on the experimental snapshots.

size range of 1.0–$1.5\,\mathrm{mm}$ (Mo-Sci GL0191SB/1000-1500).

The porosity of the packed cell is the ratio of the volume of fluid in the cell to the bulk internal volume of the cell. From four measurements, we find that the mean porosity of the packed cell is $\phi = 0.388$ with a standard deviation of 0.002. This is consistent with the expected porosity of a poured random packing of monodisperse spheres. Because we disassemble, clean, reassemble, and repack the cell after each measurement, the small standard deviation indicates that the properties of the packed cell are sufficiently consistent across experiments.

We measure the effective permeability of the packed cell directly by treating it as a fitting parameter: when comparing the model to an experiment for a buoyant current without convective dissolution ($q_d = 0$), this is the only unknown quantity. Since we expect the properties of the packed cell to be consistent across experiments, we fit the permeability for one experiment and use this same value for all other experiments, with and without convective dissolution. We find the permeability of the packed cell to be $k = 9.5 \times 10^{-10}\,\mathrm{m}^2$. For comparison, the Kozeny-Carman relation for the permeability of a packed bed of monodisperse spheres predicts, for the same nominal diameter and porosity, a permeability of $13.5 \times 10^{-10}\,\mathrm{m}^2$, or about 50% larger. That our measured value is somewhat lower than the prediction is consistent with the fact that our beads are not monodisperse.

We also conduct experiments in a Hele-Shaw cell. The materials and methods are the same except that we replace the middle spacer with a thinner one so that the working area has a thickness of about 1.4 mm. The porosity of a Hele-Shaw cell is $\phi \equiv 1$. We measure the effective permeability of the Hele-Shaw cell to be $0.95 \times 10^{-7}\,\mathrm{m}^2$, which compares well with the estimated value of $b^2/12 = 1.6 \times 10^{-7}\,\mathrm{m}^2$ for a Hele-Shaw cell of thickness $b = 1.4\,\mathrm{mm}$.

To perform an experiment, we orient the packed flow cell "vertically" (long direction aligned with gravity) and inject the dense fluid from the bottom. We then add the buoyant fluid via an injection port at the top, close all ports, and rotate the cell to the desired orientation (an angle ϑ from horizontal) to initiate the fluid flow. We record the experiment with a digital still camera. From the resulting images, we measure the position of the leading edge or "nose" of the current as a function of time.

Comparing the model with the water-PG experiments requires determining one additional parameter: the rate of convective dissolution q_d. Recent numerical and experimental work has shown that q_d is approximately constant on average [1; 4–9]. We are unable to measure this rate directly in our migrating-current experiments because we do not perform a concentration-to-light-intensity calibration. Instead, we measure this rate via an independent experiment in the packed flow cell for a stationary layer of water overlying PG. To do so, we leave the flow cell in the vertical orientation (long direction aligned with gravity) after adding the buoyant fluid. The rate at which the water-PG interface retreats is a direct measurement of the rate of convective dissolution [1; 7]. We measure this rate to be $q_d = 7.0 \times 10^{-8}\,\mathrm{m/s}$. The rate of convective dissolution has dimensions of length per time because it is the volume of buoyant fluid dissolved per unit interfacial area per unit time. The dissolving interface retreats at velocity q_d/ϕ. Although measured for a stationary layer, we assume that this dissolution rate applies also to a migrating current. High-resolution numerical simulations offer a promising avenue for assessing the validity of this assumption.

We compare the nose positions measured experimentally with those predicted by the model [Eq. (1)] in Fig. 2 of the main text. The model also captures the evolution of the shape of the buoyant current (Figure S2).

Mathematical model with capillary and solubility trapping. We have elsewhere developed and discussed a sharp-interface model for the macroscopic evolution of a buoyant current of CO_2 in a sloping aquifer with a net groundwater through-flow, subject to residual and solubility trapping [10].

In developing the model, we have neglected capillarity and assumed vertical flow equilibrium. The assumption of negligible capillarity is justified when the capillary pressure is small relative to typical viscous and gravitational pressure changes in the flow. While capillarity may have some macroscopic impact on the evolution of the buoyant current [11–13], the focus of this study is on the impact of convective dissolution, and we do not expect capillarity to have a qualitative impact on the results presented here. The assumption of vertical flow equilibrium involves neglecting the vertical component of the fluid velocity relative to the horizontal one, which requires that the buoyant current is thin relative to its length. This assumption is not met in our experiments at early times since we use an initial condition that is roughly square (Fig. S2), but rapidly becomes valid as the current lengthens and thins. We estimate that vertical flow becomes negligible when the dimensionless length of the current is greater than about 3 [14; 15], which occurs at very early times in our experiments (Fig. 2).

With no net fluid flow through the cell, the model takes the form

$$\widetilde{\mathcal{R}}\frac{\partial h}{\partial t} + \kappa\frac{\partial}{\partial x}\left[\sin\vartheta\,(1-f)h - \cos\vartheta\,(1-f)h\,\frac{\partial h}{\partial x}\right] = -\widetilde{\mathcal{R}}\,q_d/\phi, \tag{S1}$$

with

$$\widetilde{\mathcal{R}} = \begin{cases} 1 & \text{if} \quad \partial h/\partial t > -q_d/\phi, \\ 1-\Gamma & \text{otherwise,} \end{cases} \tag{S2}$$

where $\Gamma = S_{gr}/(1-S_{wc})$ is the residual trapping number and the other parameters are as defined in the main text. The conditional coefficient $\widetilde{\mathcal{R}}$ accounts for residual trapping by taking a value of 1 on portions of the interface that are in drainage (where CO_2 displaces water) and a value of $\Gamma \leq 1$ on portions that are in imbibition (where water displaces CO_2, and blobs of CO_2 are left behind). When there is no residual trapping, $\Gamma \equiv 1$ and Eq. (S1) reduces to Eq. (1) of the main text.

We solve Eq. (S1) for the interface height h in the half-space $x \geq 0$, subject to the Neumann boundary conditions ($\partial h/\partial x = 0$) at the ends of the cell and for an initial condition that approximates the step function $h(x, t = 0) = 1$ for $x < 1$ and $h(x, t = 0) = 0$ for $x > 1$. Although Eq. (S1) can be solved analytically in some limits [10], we solve it numerically in general using a finite-volume method in space with explicit time integration.

Estimation of parameters for the Mt. Simon Sandstone. As discussed in §5, we consider a migrating current of CO_2 in the Mt. Simon sandstone (Region a as discussed in §S5.1 of [16]). We assume that $M = 10$ Gt of CO_2 are injected uniformly along a linear array of wells of length $W = 200$ km. This is about one-half of the pressure-constrained capacity of this formation, which [16] estimated as about 23 Gt of CO_2 injected over about 100 years [16, Figure 3 and Table S23].

We estimate $\mathcal{M}$, N_s, and N_d for this scenario using parameters from [16, Table S2]. We report the relevant parameters here in Table S1. We use a conservative value of the residual trapping number $\Gamma \approx 0.2$ and consider angles ranging from 0 to 2 degrees. The actual slope of this aquifer is $\vartheta_{\rm true} \approx 0.5^\circ$ and we can estimate $\Gamma_{\rm true} \approx S_{gr}/(1-S_{wc}) = 0.5$.

Parameter	Value
ρ_g	$700\ \mathrm{kg \cdot m^{-3}}$
ρ_w	$1000\ \mathrm{kg \cdot m^{-3}}$
μ_g	$6 \times 10^{-5}\ \mathrm{Pa \cdot s}$
μ_w	$8 \times 10^{-4}\ \mathrm{Pa \cdot s}$
k	$1 \times 10^{-13}\ \mathrm{m^2}$
ϕ	0.2
H	$400\ \mathrm{m}$
ϑ	0.5°
S_{gr}	0.3
S_{wc}	0.4
χ_v	0.05
α	0.01
$\Delta\rho_d$	$6\ \mathrm{kg \cdot m^{-3}}$

Table S1. Parameters for Region a of the Mt. Simon sandstone from Table S2 of [16]. See §S5.1 and Table S2 of [16] for more details.

From these parameters, we calculate $\Delta\rho = \rho_w - \rho_g = 300\ \mathrm{kg \cdot m^{-3}}$ and $\kappa = \Delta\rho\, gk/\phi\mu_g = 2.5 \times 10^{-5}\,\mathrm{m/s}$. The characteristic initial width of the CO_2 plume is $L = M/(\rho_g \phi H W) \approx 890\,\mathrm{m}$ and the characteristic time is $T = L^2/(H\kappa\cos\vartheta) \approx 8.1 \times 10^7\,\mathrm{s}$. We estimate the dissolution flux to be $q_d = \alpha\chi_v\Delta\rho_d g k/\mu_w \approx 3.7 \times 10^{-12}\,\mathrm{m/s}$, where $\chi_v \approx 0.05$ is the maximum equivalent volume of free-phase CO_2 that can dissolve in one unit volume of groundwater, corresponding to a maximum solubility of mass fraction $\chi_m = \rho_g\chi_v/(\rho_w + \Delta\rho_d) \approx 0.035$ [10, §3.2]. We then have that $\mathcal{M} = \mu_w/\mu_g \approx 13$, $N_d = L^2 q_d/(H^2\phi\kappa\cos\vartheta) \approx 3.7 \times 10^{-6}$, and $N_s = (L/H)\tan\vartheta \approx 0$ to 0.078 for angles ranging from 0 to 2 degrees.

Supporting References

S1. S. Backhaus, K. Turitsyn, and R. E. Ecke. Convective instability and mass transport of diffusion layers in a Hele-Shaw geometry. *Physical Review Letters*, 106(10):104501, 2011.

S2. Dow Chemical. Propylene glycols - density values, 2011. https://dow-answer.custhelp.com/app/answers/detail/a_id/7471.

S3. Dow Chemical. Propylene glycols - viscosities of aqueous solutions, 2011. https://dow-answer.custhelp.com/app/answers/detail/a_id/7472.

S4. J. Hidalgo and J. Carrera. Effect of dispersion on the onset of convection during CO_2 sequestration. *Journal of Fluid Mechanics*, 640:441–452, 2009.

S5. T. J. Kneafsey and K. Pruess. Laboratory flow experiments for visualizing carbon dioxide-induced, density-driven brine convection. *Transport in Porous Media*, 82(1):123–139, 2010.

S6. G. S. H. Pau, J. B. Bell, K. Pruess, A. S. Almgren, M. J. Lijewski, and K. Zhang. High-resolution simulation and characterization of density-driven flow in CO_2 storage in saline aquifers. *Advances in Water Resources*, 33(4):443–455, 2010.

S7. J. A. Neufeld, M. A. Hesse, A. Riaz, M. A. Hallworth, H. A. Tchelepi, and H. E. Huppert. Convective dissolution of carbon dioxide in saline aquifers. *Geophysical Research Letters*, 37:L22404, 2010.

S8. J. J. Hidalgo, J. Fe, L. Cueto-Felgueroso, and R. Juanes. Scaling of convective mixing in porous media. *Physical Review Letters*, 109(26):264503, 2012.

S9. A. C. Slim, M. M. Bandi, J. C. Miller, and L. Mahadevan. Dissolution-driven convection in a Hele-Shaw cell. *Physics of Fluids*, 25:024101, 2013.

S10. C. W. MacMinn, M. L. Szulczewski, and R. Juanes. CO_2 migration in saline aquifers. Part 2. Capillary and solubility trapping. *Journal of Fluid Mechanics*, 688:321–351, 2011.

S11. J. M. Nordbotten and H. K. Dahle. Impact of the capillary fringe in vertically integrated models for CO_2 storage. *Water Resources Research*, 47:W02537, 2011.

S12. M. J. Golding, J. A. Neufeld, M. A. Hesse, and H. E. Huppert. Two-phase gravity currents in porous media. *Journal of Fluid Mechanics*, 678:248–270, 2011.

S13. B. Zhao, C. W. MacMinn, M. L. Szulczewski, J. A. Neufeld, H. E. Huppert, and R. Juanes. Interface pinning of immiscible exchange flows in porous media. *Physical Review E*, 87:023015, 2013.

S14. Y. C. Yortsos. A theoretical analysis of vertical flow equilibrium. *Transport in Porous Media*, 18(2):107–129, 1995.

S15. R. de Loubens and T. S. Ramakrishnan. Analysis and computation of gravity-induced migration in porous media. *Journal of Fluid Mechanics*, 675:60–86, 2011.

S16. M. L. Szulczewski, C. W. MacMinn, H. J. Herzog, and R. Juanes. Lifetime of carbon capture and storage as a climate-change mitigation technology. *Proceedings of the National Academy of Sciences of the United States of America*, 109(14):5185–5189, 2012.